Springer

KSME

Journal of Mechanical Science and Technology 32 (12) (2018) 5749~5754
www.springerlink.com/content/1738-494x(Print)/1976-3824(Online)
DOI 10.1007/s12206-018-1122-8

The application of aerodynamic brake for high-speed trains †

MinKyo Lee and Binayak Bhandari*

Department of Railroad Integrated System Engineering, Woosong University, 171 Dongdaejeon-ro, Dong-gu, Daejeon, Korea

(Manuscript Received June 22, 2018; Revised August 31, 2018; Accepted September 30, 2018)

Abstract

The braking distance for high-speed trains (HST) operating over 200 km/h takes roughly over 6000 m and 1 minute 40 seconds. In an emergency situation, both braking distance and stopping time are too high. Reducing the time and the distance for braking for such trains will be beneficial for passengers' safety and railway system management. A number of studies have been conducted to develop a better braking system based on mechanical or electromechanical technologies to overcome this issue. In this study, computational fluid dynamics (CFD) analysis are conducted by designing prototypes of aerodynamic brakes inspired by commercial aircrafts' flaps. Limited studies have been performed in implementing an aerodynamic brake in the high-speed trains. The primary emphasis of this study is to examine the argumentation on an aerodynamic performance by mounting the aerodynamic brake on HSTs to find out its effectiveness in terms of energy saving. A full-scale model of HST was analyzed in this study by varying velocities (200 km/h to 400 km/h), and the operating angles (35° to 55°). The results show that aerodynamic brakes can reduce the braking distance by 2.53 % and 1.56 % for when using the commercial and emergent braking, respectively.

Keywords: High-speed trains; Aerodynamic brake; CFD; Drag coefficient

1. Introduction

Brake distance of trains varies depending on assorted factors such as the free running distance, the maximal speed or the performance of braking devices involving the pneumatic brake, disk brake or regenerative brake. It is one of the most important issues when it comes to passengers' safety and their convenience and to the efficiency of railway management; therefore, an advanced braking system is required corresponding to the improvement of the speed of trains. Since the high-speed trains (HSTs) has become a major transportation mode for the public, this issue has become more important than before. In addition, due to HSTs characteristics, more efforts of power and time to decelerate them are required especially for when they are running at their maximum speed. Thus, minimizing the brake distance will bring profitable outcomes such as an increase of the rail capacity, the accuracy of arrival time, and ultimately the passengers' safety.

Commercial aircraft have an efficient streamlined design. Similar to aircraft, HSTs are also designed in extremely streamlined shape to reduce drag, because faster vehicles are more affected by the air friction [1]. However, it takes longer distance and time compared to conventional train to stop HST because of high-speed and streamlined design. In order to mitigate this problem, a mechanism is to be designed to increase the drag force by deploying them during stopping of the train.

Various studies have been conducted regarding the relationship between the HSTs and aerodynamic behaviors around them such as pressure field [2], aerodynamic noise [3, 4], streamlined shape [5-7], slipstream [8, 9]; however, to the authors' knowledge, the research related to the aerodynamic braking system and its efficiency in terms of energy saving in a real situation have been rarely examined. Motivated by the aircraft aerodynamic brake design, in this research an aerodynamic brake was designed for HSTs with the intention to raise the drag force while also increasing the rolling resistance to lower the total braking distance and to save energy. This study numerically analyzes in detail on an aerodynamic brake device, its aerodynamic performance and proposes its application in high-speed trains based on CFD results.

2. The aerodynamic brake simulation model

2.1 Geometrical model

This study uses a full-scaled HST model for the computational analysis. The train model consists of two power cars with cab and two trailers as shown in Fig. 1. Since this paper focuses on the overall aerodynamic behaviors around the brake, other detailed components such as pantographs, wipers, and bogies were not taken into consideration in this study. The

*Corresponding author. Tel.: +82 42 630 9898, Fax.: +82 42 630 9708
E-mail address: binayak@sis.ac.kr
† Recommended by Associate Editor Seongwon Kang

Table 1. Parameters of the model train.

Parameters	Size (m)
Length	89
Width	4.1
Height	3.2

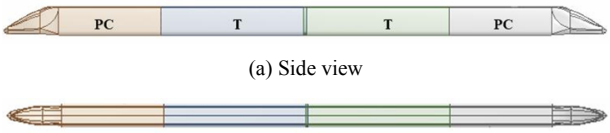

(a) Side view

(b) Top view

Fig. 1. Full-scaled HST model.

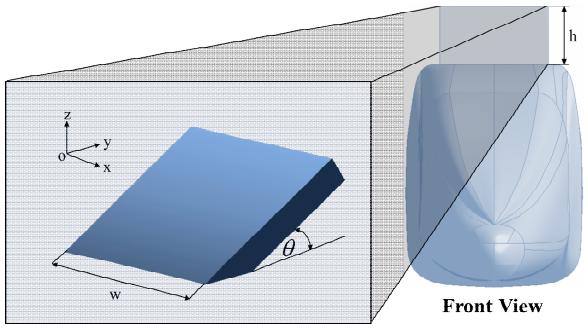

Fig. 2. The aerodynamic brake and its application for HSTs.

detailed parameters of the model train are as shown in Table 1.

The aerodynamic brakes are mounted on the top surface of the HST that can be operated to spoil the airflow. Air brake mechanism has a retractable panel mechanism intended to intentionally increase in drag component of a streamlined HST design in a controlled way. The mechanism is designed in such a way that it will always be operated below the catenary system and thus avoid electric related accidents.

The intended application of the aerodynamic brake on the HST is as shown in Fig. 2. The dimensions of the aerodynamic and its operating angles have been chosen as shown in Table 2 in consideration of the distance between the trolley wires and the trains, and the vehicle and construction clearance based on the standard specifications of Republic of Korea.

2.2 Computational domain and boundary conditions

The solver utilized for the CFD simulation is a commercial code CFX of ANSYS 15. The computational domain for the simulations has been depicted as shown in Fig. 3. The model dimensions are as follows: L = 89 m, W = 4.1 m and H = 3.2 m along x -, y - and z - directions, respectively. The computational domain has dimensions of 5 L × 11 H × 27 W. The distance between the nose of the head train and the inlet boundary is 1 L, and the distance between the nose of the rear head train and the outlet boundary is 3 L.

Since the origin of the coordinate system is positioned at the center of the train, the distance from the train to both side boundaries is 13.5w and the distances between the bottom of the train and the ground are the same as 0.1 m.

Table 2. Dimensions of an aerodynamic brake.

Case	w (mm)	h (mm)	Angle (°)
(1)	-	740	35
(2)	2000	910	45
(3)	-	1200	55
(4)	-	-	N B

The inflow boundary is assigned an inlet velocity ranging from 200 km/h to 400 km/h at 50 km/h steps. The outflow boundary is assigned an outlet condition corresponding to a gauge pressure of 0 Pa, and the reference pressure is set to 1 atm. The left, right and top sides are defined as no-slip walls. And the bottom side is defined as moving wall with an equivalent speed with the running speed of the train to achieve the ground effect. Among the various formulations for solving turbulent flow problem, k-ε and k-ω are most popular turbulence model.

Although k-ω (SST) is good for strong curvature, separated flows and jets it is computationally more expensive and difficult to converse. Selected cases were studied using both k-ε (SKE) model and k-ω (SST) model and found that the results were within ± 5 %. Thus, in this study k-ε (SKE) model was used because of its good convergence rate and relatively low memory requirements and its good performance for external flow problems around complex geometries. The standard k-ε model (SKE) can be expressed as follows:

For turbulence kinetic energy k

$$\frac{\partial(\rho k)}{\partial t}+\frac{\partial(\rho k u_i)}{\partial x_i}=\frac{\partial}{\partial x_j}\left[\frac{\mu_t}{\sigma_k}\frac{\partial k}{\partial x_j}\right]+2\mu_t \mathrm{E}_{ij}\mathrm{E}_{ij}\,. \tag{1}$$

For dissipation rate ε

$$\frac{\partial(\rho\varepsilon)}{\partial t}+\frac{\partial(\rho\varepsilon u_i)}{\partial x_i}=\frac{\partial}{\partial x_j}\left[\frac{\mu_t}{\sigma_\varepsilon}\frac{\partial \varepsilon}{\partial x_j}\right]+C_{1\varepsilon}\frac{\varepsilon}{k}2\mu_t \mathrm{E}_{ij}\mathrm{E}_{ij}-C_{2\varepsilon}\rho\frac{\varepsilon^2}{k} \tag{2}$$

where u_i is the velocity component in a corresponding direction, E_{ij} is the component of the rate of deformation, and μ_t is the eddy viscosity. The dissipation rate is related to k and a turbulence length scale as expressed below.

$$\varepsilon \approx \frac{k^{2/3}}{L_t}\,. \tag{3}$$

2.3 Grid independent study

The grid independent study was performed using a different number of tetrahedral meshes combined with prism layers on

Table 3. Mesh refinement case study.

Test case #	No. of mesh (million)	First layer thickness (mm)	No. of prism layers	Operation angle (°)	Train speed (km/h)	C_D
1	4.04	0.003	10	35	200	0.2238
2	5.94	0.003	10	35	200	0.2236
3	8.06	0.003	10	35	200	0.2235

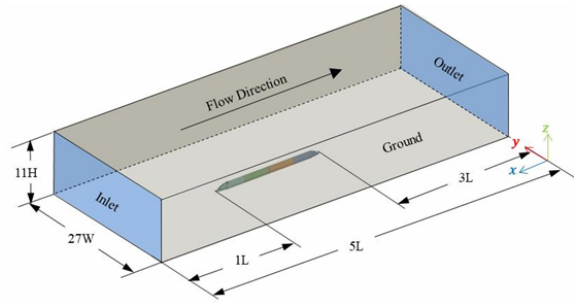

Fig. 3. The flow-field computational domain.

the surface of the train to capture the boundary layers, and the meshes around the wake regions are more refined to assess the influence of different meshes on the computation. Using the scalable wall function with the k-ε model to capture the near wall velocity profile, it was considered to keep the y^+ value within the desired range ($30 < y^+ < 300$) meaning a proper first layer thickness had to be calculated accordingly [10, 11]. Three types of mesh configurations were tested with 10 prism layers of a first layer thickness that satisfies the appropriate wall spacing required for the wall treatment as the y plus value is set within 30 to 300 as a rule of thumb. The parameters of three types of mesh configurations and the corresponding computational results are listed in Table 3.

The drag coefficient (C_D) obtained from the first mesh configuration has a slightly higher value than the second and the third mesh type. The value between the first mesh and the second mesh only differs around by 0.0002, and it differs by 0.0003 between the first and the third mesh type. Thus, it is reasonable to conclude that using the mesh with the minimum number is the most cost-effective. Accordingly, the first mesh configuration was chosen for the entire simulation cases to minimize the resources and time required for the computation.

The distribution of the mesh is presented as shown in Fig. 4.

2.4 Simulation cases

The simulation cases consist of three different sections depending upon the operational angle of the aerodynamic brake and the running speed of the train set 200 km/h corresponding to the definition of high-speed trains.

For each operation angle of the aerodynamic brake, velocities were set from 200 km/h to 400 km/h. The Reynolds number of the aerodynamic brake corresponding to each operation angle and the running speed of the train are shown in Table 4.

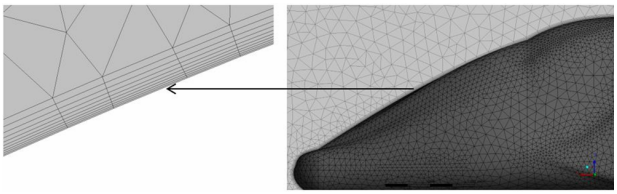

Fig. 4. The mesh distribution.

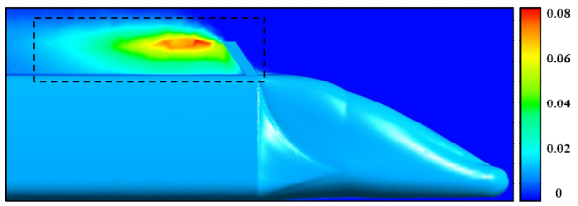

(a)

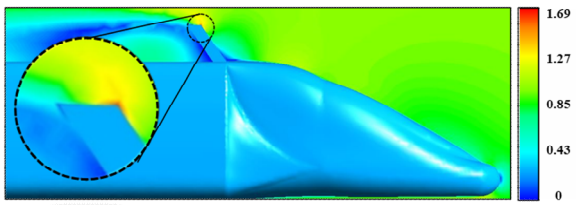

(b)

Fig. 5. (a) TKE; (b) velocity distribution at the front edge of the aerodynamic brake.

3. Results and discussion

3.1 CFD simulation results

The solution converged with the residual values of 1E-05 is generally considered as well converged solution. The effects of the aerodynamic brake around the train are very noticeable compared to the simulation without the brake. The turbulence starts occurring at the edge of the aerodynamic brake due to the flow separation, and substantial turbulent kinetic energy (TKE) is clustered on the wake region, i.e., right behind the aerodynamic brake. It is also observed that the velocity of flow is extremely high at the front edge of the aerodynamic brake. Fig. 5 shows the TKE and velocity distribution by normalizing the velocity of the train (V_{max} = 111.1 m/s) in the wake region at 55° operating angle and 400 km/h running speed.

Furthermore, it is observed that the pressure near the aerodynamic brake increases significantly due to the wind speed; therefore, the drag force is expected to increase accordingly.

Table 4. Reynolds number corresponding to each simulation case.

Operation angle (°)	Chord length (m)	Reynolds number				
		V_0 = 200 km/h	250 km/h	300 km/h	350 km/h	V_{max} = 400 km/h
35	1.52	5.52E+06	6.89E+06	8.27E+06	9.65E+06	1.10E+07
45	1.37	4.99E+06	6.23E+06	7.48E+06	8.72E+06	9.97E+06
55	1.15	4.17E+06	5.21E+06	6.26E+06	7.30E+06	8.34E+06

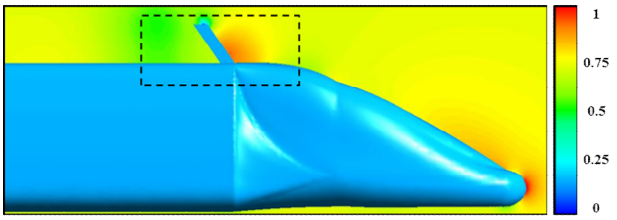

Fig. 6. Normalized pressure distribution near the aerodynamic brake at 55° operating angle and 400 km/h running speed.

The normalized pressure distribution featuring from 0 to 1 near the aerodynamic brake system is shown in Fig. 6.

Fig. 7 shows the wake region behind the aerodynamic brake at different operating angles. A wake region is generally expected to happen behind a blunt body; however, it is difficult to predict the exact size or the position of wake region empirically. Locating wake region will be helpful for minimizing the potential risks of heavy loads by wind, and also for optimizing the shape and the position of the aerodynamic brake for avoiding damage to equipment like overhead lines and pantographs. The results show that the turbulent wake region behind the aerodynamic brake becomes thicker as higher operating angles bring the separation point towards the nose of the train. However, the position of the turbulent wake region does not change a lot along *x*-axis when increasing the operating angle by 10° each time. Accordingly, the total width of the wake region behind the aerodynamic brake may become thicker as the operating angle increases; however, the variation does not seem to be very noticeable.

In this study, the drag coefficient for each case was calculated to examine the effectiveness of the aerodynamic brake. The drag coefficient can be calculated as follow:

$$C_D = \frac{2F_D}{\rho A U^2} \tag{4}$$

where F_D is drag force; A is the cross-sectional area normal to the flow direction, which is listed in Table 5, ρ is the air density, which is approximately 1.2 kg/m^3 and U is the wind speed which varies from V_0 (200 km/h) to V_{max} (400 km/h).

Fig. 8 shows the comparison of the drag forces with/without aerodynamic brake engaged. A high drag force results in a sharper slope. For the 400 km/h case, there is a significant increase in drag force thus has sharper slope compared to the gradual slope at lower operating speed. It can be noticed that the increase in drag force for all cases are non-linear and increases as the speed increases.

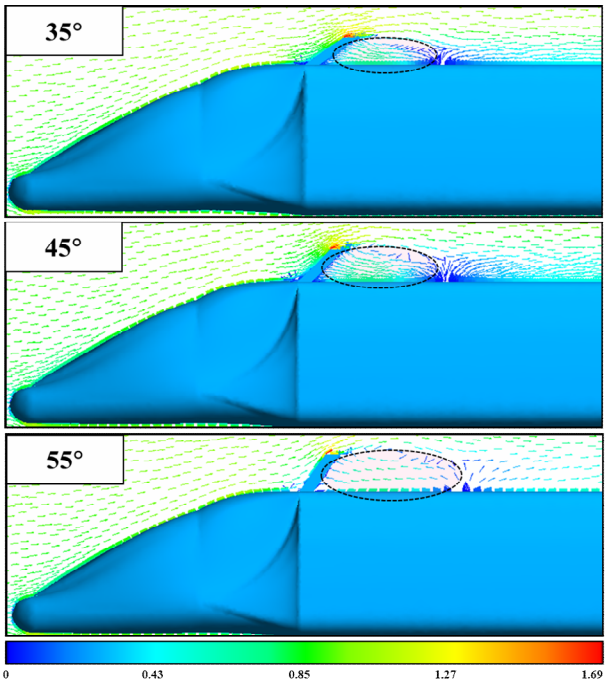

Fig. 7. Turbulent wake region behind the aerodynamic brake at different operating angles from 35° to 55°.

In addition, it can be seen in Fig. 9 that the gap between the case of NB and each operating angle widens noticeably as the velocity increases.

Lastly, to find out the aerodynamic impact of the aerodynamic brake, the drag coefficients by different operating angles at the case of 400 km/h are presented in Fig. 10. It can be seen that the drag coefficient at NB (0.18), increase to 0.26, at 55° operating angle, an increase of 30 %.

3.2 Discussion

To find the effectiveness of the aerodynamic brake, the variation of the braking distance was calculated. The braking distance of trains can be found by integrating the longitudinal kinematic equation, which can be expressed as Eq. (5).

$$m\frac{dv}{dt} = F_B + F_D + F_R + F_G + F_C \tag{5}$$

where m is the mass of the trains, F_B is the braking force of the

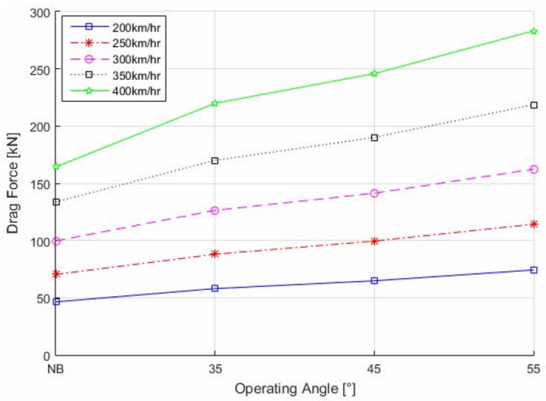

Fig. 8. Variation of drag force at different operating angles from NB to 55°.

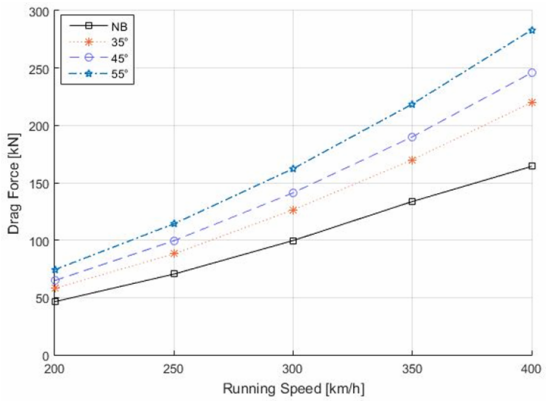

Fig. 9. Variation of drag force at different running speed from NB to 450 km/h.

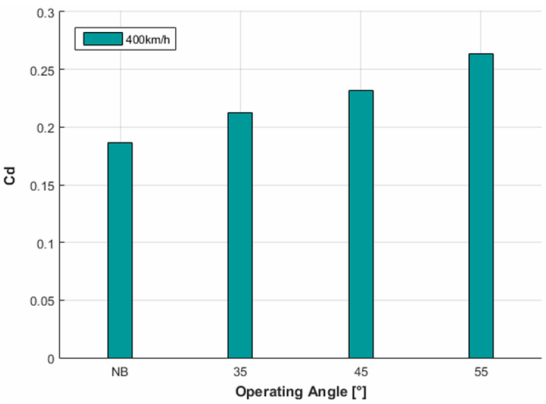

Fig. 10. The drag coefficient of the case 400 km/h at different operating angles from NB to 55°.

locomotives, F_D is the drag resistance, F_R is the rolling resistance, F_G is the gradient resistance, and F_C is the curve resistance. In this study, other factors except for the braking force, the air resistance, and the rolling resistance were ignored to simplify the calculation. The braking force (F_B) differs following the deceleration rate. Korean HSTs generally have declaration rates of 2.1 km/h/s and 3.6 km/h/s for both commercial and emergent purposes, respectively. The braking force (F_B) of rolling stocks can be obtained by Eq. (6).

$$F_B(kgf) = 28.35 \times \alpha_B \times (m_E \times 1.1 + m_P) \quad (6)$$

where α_B the deceleration, m_E is the mass of the train without loads in tons, and m_P is the mass of passengers in tons. As to compensate the inertia mass, a factor of 1.1 is multiplied to the mass of the train without loads (m_E).

It is seen that the total braking distance of a train running at 400 km/h can be reduced up to 2.53 % in a general situation and 1.56 % in an emergent situation with the aerodynamic brake by operating it at 55° for both cases.

Assuming the efficiency of the motor to be 60 %, the electric power produced by the regenerative braking can be simply calculated by considering the initial kinetic energy of trains and braking time. As a result, 140 kW can be saved every time a HST starts braking at 400 km/h due to the decrease of braking time. In average 100 HST operates daily from Seoul to Busan in the Kyung-Bu line in South Korea during the weekdays [12]. HSTs has stoppage in large metropolis as Seoul, Daejeon, Daegu, and Busan, considering these cases, the total amount of energy saving per year by applying the aerodynamic brake is around 15.33 GW.

The above result is for the case using just one aerodynamic brake in the HST, however, such aerodynamic brakes can be operated in cascades throughout the length of the train. It can be intuitively expected that such system will drastically help in reducing the braking distance.

Thus, more attention is needed to investigate the operating angle of aerodynamic brake as well as the detailed mechanism of its implementation to the existing HSTs taking practical considerations of limited space, operating speed and aerodynamic brake design. Developing suitable mathematical models would be an important piece of work within this line of research.

4. Conclusions

An aerodynamic brake for high-speed trains (HSTs) inspired by the aerodynamic brakes of commercial airplanes is proposed in order to improve the braking system of HSTs. The CFD simulation was conducted to figure out its aerodynamic behavior. The main emphasis is to examine the aerodynamic effectiveness of the aerodynamic brake and on the comparison among drag coefficients obtained by each simulation.

The flow separation caused by the aerodynamic brake mainly depends on the operating angle; therefore, it is recommended to operate it at its maximal angle within the extent that allows the aerodynamic brake to stay at stable condition despite the high running speed. The increase in drag coefficient by implementing the aerodynamic brake in HST can find its application in reducing the braking distance, braking time as well as reducing energy consumption or saving energy by roughly 15.33 GW.

Acknowledgments

This research was supported by Basic Science Research Program through the National Research Foundation of Korea (NRF) funded by the Ministry of Education (2017R1D1 A1B03034437).

References

[1] S. J. Byun, S. Cry and S. W. Kim, Numerical simulation of aerodynamic drag for high-speed train using LBM, *Journal of the Korean Society for Railway*, 5 (2014) 1660-1665.

[2] H. B. Kwon, S. W. Nam and C. W. Cha, A numerical analysis on the pressure field around KTX train using the standard framework of CFD analysis for railway system, *Journal of the Korean Society for Railway*, 5 (2006) 1-6.

[3] Y. Zhang, J. Zhang, T. Li, L. Zhang and W. Zang, Research on aerodynamic noise reduction for high-speed trains, *Shock and Vibration*, 2016 (2016) 1-21.

[4] C. Paz, E. Suárez, C. Gil and M. Concheiro, Numerical study of the impact of windblown sand particles on a high speed train, *Journal of Wind Engineering & Industrial Aerodynamics*, 145 (2015) 89-93.

[5] G. Xu, X. Liang, S, Yao, D. Chen and Z. Li, Multi-objective aerodynamic optimization of the streamlined shape of high-speed trains based on the Kriging model, *PLoS ONE,* 12 (1) (2017) e0170803, https://doi.org/10.1371/journal.pone.0170803.

[6] M. H. Kwak, S. W. Yun and C. S. Park, Nose shape optimization of high-speed train for the consideration of crosswind stability, *Journal of the Korean Society for Railway*, 10 (2015) 1341-1345.

[7] X. Yang, J. Jin and G. Shi, Preliminary study on streamlined design of longitudinal profile of high-speed train head shape, *13th COTA International Conference of Transportation Professionals*, 13 (2013) 1469-1476.

[8] S. H. Yun, M. H. Park, S. W. Nam and C. S. Park, Research for aerodynamic drag reduction method of KTX San-chon, *Journal of the Korean Society for Railway*, 5 (2015) 166-171.

[9] S. Wang, J. R. Bell, D. Burton, A. H. Herbst, J. Sheridan and M. C. Thompson, The performance of different turbulence models (URANS,SAS and DES) for predicting high-speed train slipstream, *Journal of Wind Engineering & Industrial Aerodynamics*, 165 (2017) 46-57.

[10] S. W. Kim, A near-wall turbulence model and its application to fully developed turbulence cannel and pipe flows, *NASA Technical Memorandum 101399*, USA (1988).

[11] Z. T. Ai and C. M. Mak, Potential use of reduced-scale models in CFD simulations to save numerical resources: Theoretical analysis and case study of flow around an isolated building, *Journal of Wind Engineering & Industrial Aerodynamics*, 134 (2014) 25-29.

[12] Korea Railroad Corporation, *Train time*, Retrieved from http://www.letskorail.com/ebizcom/cs/guide/guide/guide11.do (2018).

MinKyo Lee is an undergraduate student majoring in railroad engineering at the Department of Railroad Integrated Systems Engineering, Woosong University. His interests in research include numerical simulations, developing prosthetic devices using haptics & artificial intelligence.

Binayak Bhandari is currently a Department Head of Railroad Integrated Systems Engineering at Woosong University, Daejeon, Korea. Dr. Bhandari received his Ph.D. from Seoul National University (SNU), Mechanical and Aerospace Engineering in 2014. He worked as Post-doctoral fellow in SNU for one year and joined Woosong University as Assistant Professor in 2015. Dr. Bhandari focuses on Computational Analysis of high-speed trains, fatigue of rail, vibration and dynamics, Micro/Nano fabrication, 3D Printing, Smart Material, Artificial Intelligence, Computer Vision, Renewable Energy and Appropriate Technology.